JACS
JOURNAL OF THE AMERICAN CHEMICAL SOCIETY
Article
pubs.acs.org/JACS

Iron(III)-Doped, Silica Nanoshells: A Biodegradable Form of Silica

Kristina K. Pohaku Mitchell,[†] Alexander Liberman,[‡] Andrew C. Kummel,[†] and William C. Trogler*[,†]

[†]Department of Chemistry and Biochemistry, [‡]Department of Materials Science and Engineering, University of California San Diego, 9500 Gilman Drive, La Jolla, California 92093, United States

Supporting Information

ABSTRACT: Silica nanoparticles are being investigated for a number of medical applications; however, their use *in vivo* has been questioned because of the potential for bioaccumulation. To obviate this problem, silica nanoshells were tested for enhanced biodegradability by doping iron(III) into the nanoshells. Exposure of the doped silica to small molecule chelators and mammalian serum was explored to test whether the removal of iron(III) from the silica nanoshell structure would facilitate its degradation. Iron chelators, such as EDTA, desferrioxamine, and deferiprone, were found to cause the nanoshells to degrade on the removal of iron(III) within several days at 80 °C. When the iron(III)-doped, silica nanoshells were submerged in fetal bovine and human serums at physiological temperature, they also degrade via removal of the iron by serum proteins, such as transferrin, over a period of several weeks.

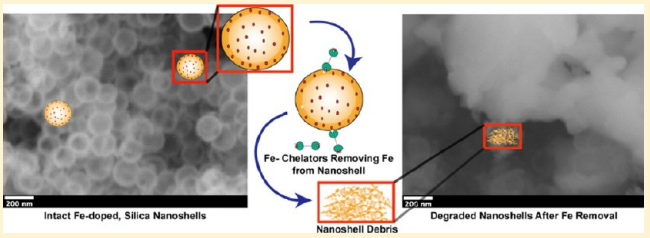

INTRODUCTION

Silica nanoparticles are being investigated for a variety of applications, such as catalysis, ultrasound contrast imaging agents, photonic band gap materials, adsorptive materials, and drug delivery.[1−8] There are several characteristics that are desirable for materials to be used in drug delivery: a long shelf life, facile commercial synthetic scale up, and clearance from the body. Calcined silica is a potential nanoporous material for biomedical applications because it is a robust, chemically inert material of high surface area whose surface chemical properties are easily modified. However, the stability of silica makes it problematic for *in vivo* medical applications because of the potential of inert nanoparticles to bioaccumulate.[9] Mesoporous silica nanoparticles have been found to accumulate in the liver, kidneys, bladder, and spleen with a small fraction of nanoparticles also found in the lungs.[10−15] The location of accumulation depends, however, on the size, shape, and surface properties of the nanoparticles.[11−15] Industrial uses of nanosilica also suffer from the occupational hazard that it poses, since inhalation may lead to silicosis.[16−18] Therefore, methods that increase the biodegradable nature of silica could have a wide impact in mitigating potential hazards with its use.

The rate at which silica degrades depends on a number of factors including composition, preparation, calcination temperature, surface area, and pore structure.[13,19−22] Many studies have looked at using various forms of silica-based materials (xerogels, sols, bioactive glasses, etc.) as biocompatible, biodegradable materials.[20,21,23−28] Of the materials studied, compounds that had been calcined, or sintered, at high temperatures reduced the amount of silica released or dissolved from the bulk material.[13,19−22,29,30] Calcination causes the dehydration of silica and imparts it with a dense network structure. These changes to the network structure cause calcined silica to have a slow rate of degradation, thereby increasing the potential for bioaccumulation.[30] There are reports of attempts to overcome this obstacle by altering the composition of silica nanoparticles through the incorporation of cations to increase the rate at which silica degrades, for example. The incorporation of Ca^{2+} into calcined silica has been shown to increase the silica degradation rate compared to plain silica.[30] However, the mechanism of silica degradation was not clear. It was difficult to determine if the changes observed were due to the enhanced removal of silica or just the dissolution of the incorporated calcium.

This work explores the incorporation of ferric iron (Fe^{3+}) into a silica nanoshell structure. Iron, despite its large abundance, is a limiting nutrient for most forms of life due to the limited solubility of its common form, $Fe(OH)_3$, at neutral pH. As a result, nature has developed a variety of methods for the solubilization and sequestration of iron using iron chelating proteins.[31] Transferrin is an iron transport protein found in the blood serum of vertebrates.[32] Human transferrin binds iron as Fe^{3+} with a high affinity as evidenced by its dissociation constant (K_d) of 10^{-22} M at pH 7.0.[31] This strong binding affinity raised the possibility that the incorporation of Fe^{3+} into the silica structure would make silica biodegradable. Furthermore, there are clinical drugs, such as desferrioxamine and deferiprone, which are approved for chelation therapy to treat individuals with iron overload diseases, such as hemochromatosis and thalassemia. Such drugs could conceivably be administered as a secondary treatment, if necessary, to assist the removal of iron(III)-doped, silica nanoparticles.

This work explores iron(III) doping into hollow silica nanoshells prepared by the sol−gel method and polymer templating approach shown in Scheme 1.[33] Degradation of Fe-

Received: April 15, 2012
Published: August 7, 2012

   dx.doi.org/10.1021/ja3036114 | J. Am. Chem. Soc. 2012, 134, 13997−14003

Scheme 1. Synthesis of SiO_2 Nanoshells

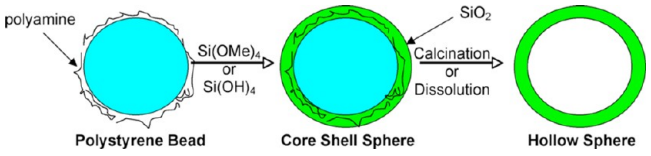

doped, hollow silica nanoshells was studied in the presence of strong iron chelates as well as in the presence of the natural chelating ligands found in mammalian serum.

EXPERIMENTAL SECTION

Materials. Tetramethoxy orthosilicate, 3-hydroxy-1,2-dimethylpyridin4(1H)-one 98% (deferiprone), desferoxamine mesylate salt 95% (desferrioxamine), ethylenediamine-tetraacetic acid disodium salt (EDTA), anhydrous ethanol, and absolute ethanol were obtained from Sigma Aldrich. The 200 nm amino polystyrene templates were obtained from PolySciences. Iron(III) ethoxide was purchased from Gelest. Heat inactivated human serum (HS) was obtained from Lonza. Fetal bovine serum (FBS) was obtained from Mediatech, Inc. All reagents were used as obtained without further purification. Scanning electron microscopy (SEM) images were acquired using a FEI/Phillips XL30 FEG ESEM with an accelerating voltage of 10 kV. Energy dispersive X-ray spectroscopy (EDS) was performed on the same instrument using the Oxford EDX attachment and INCA software. UV−vis spectroscopy was performed using a Perkin-Elmer Lambda 35 model spectrophotometer. Dynamic light scattering (DLS) and ζ potential measurements were obtained using a Malvern Zetasizer Nano ZS.

Synthesis of Iron(III)-Doped, Silica Nanoshells. A 20 mg/mL solution of iron(III) ethoxide was prepared by dissolving 20 mg of iron(III) ethoxide in 1 mL of anhydrous ethanol under an inert atmosphere. This translucent, dark-brown solution was saved until needed for synthesis of the iron(III)-doped, hollow silica nanoparticles. The particles were synthesized as follows: 1 mL of absolute ethanol and 50 μL of 200 nm amino polystyrene beads were added to a 1.5 mL microcentrifuge tube. The mixture was vortexed to suspend the polystyrene in the ethanol. As the polystyrene beads and ethanol were mixing, 3.2 μL of tetramethoxyorthosilicate (TMOS) was mixed with 10 μL of a 20 mg/mL solution of iron(III) ethoxide. When the TMOS and iron(III) ethoxide appeared to be thoroughly mixed, the translucent brown solution was added to the polystyrene bead suspension. The mixture was vortex stirred for 5 h. The nanoparticles, which appear yellow in color, were centrifuged at 7000 rpm for 5 min, the supernatant removed, and the pellet resuspended in water. This wash process was performed three times. After the last wash, the supernatant was removed, and the pellet was dried under ambient conditions. The dry pellet was removed from the microcentrifuge tube, placed in a crucible, and calcined at 550 °C in a standard muffle furnace for 18 h. An orange-brown powder was obtained from the crucible after calcination.

Nanoshell Degradation using UV−vis Spectroscopy. In water, 0.1 M aqueous solutions were prepared for disodium EDTA, desferoxamine mesylate salt, and deferiprone. A 1 mg portion of 200 nm iron(III)-doped, hollow silica nanoparticles was added to a 1.5 mL microcentrifuge tube to which 1 mL of the chelate solution was added. The samples were vortexed to suspend the particles and placed in an 80 °C water bath. From each sample, 100 μL aliquots were removed and replaced with fresh chelate solution. The aliquots were diluted with 900 μL of water, and the UV−vis spectra were obtained. Aliquots were sampled and measured every hour for a total of 8 h. After the last measurement was taken at 8 h, the suspension was left in the water bath for 16 h (a total of 24 h). Every 24 h, the samples were centrifuged, and the supernatant was removed and replaced with 1 mL of fresh chelate solution. The UV−vis spectrum was obtained for the supernatant and diluted as necessary, and the process was repeated every 24 h until there were no recoverable solids after approximately 7−10 days.

Nanoshell Degradation in Mammalian Serum. A 1 mg portion of 200 nm iron(III)-doped, hollow silica nanoparticles was placed in a 1.5 mL microcentrifuge tube. One mL of either FBS or HS was added, and the samples were vortexed to suspend the particles. The samples were placed in a 37.5 °C constant temperature water bath. The samples were vortexed every 24 h with the serum being replaced with fresh serum every third and seventh day. A pellet was isolated by centrifugation every seven days, washed twice with water, and calcined. The calcined pellets were imaged using SEM.

RESULTS AND DISCUSSION

Synthesis and Characterization of Fe-Doped, Silica Nanoshells. The synthesis of Fe-doped, hollow silica nanoparticles was adapted from the method developed by Yang et al.[33,34] As seen in Scheme 2, a polyamine was not required in the synthesis as long as amine-functionalized polystyrene (PS) beads are used as the template. Iron(III) ethoxide was dissolved in anhydrous ethanol, and the resulting solution was premixed with TMOS prior to its addition to the PS bead suspension. Water from the PS template suspension was the source of trace water for the sol−gel hydrolysis reaction to occur. The reagents are combined with the template beads and allowed to react for 5 h. The pellet is isolated by centrifugation, washed with deionized water, dried under vacuum, and then calcined. The removal of the PS core by heating to 550 °C results in the isolation of a fine powder with an orange-brown color.

Scheme 2. Synthesis of Fe-doped, Silica Nanoshells

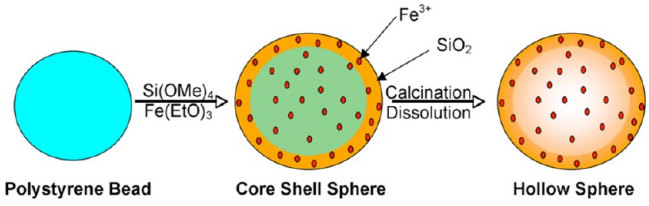

SEM was performed to determine the structure, seen in Figure 1. The SEM images reveal that the particles obtained are hollow with a continuous wall with no visible holes, cracks, or other deformations. The images also reveal that the resulting nanoshells are fairly uniform in size having an average diameter of approximately 180 nm. DLS was explored to determine the average size of the particles suspended in water. After sonication, the 200 nm Fe-doped, silica nanoshells exhibit an average diameter of 1180 nm, with a PDI of 0.54 by DLS and have a ζ potential of −48.6 mV. The DLS distribution peak, however, indicated that the mean diameters of the nanoshells measured were 318 nm. The size discrepancy observed between

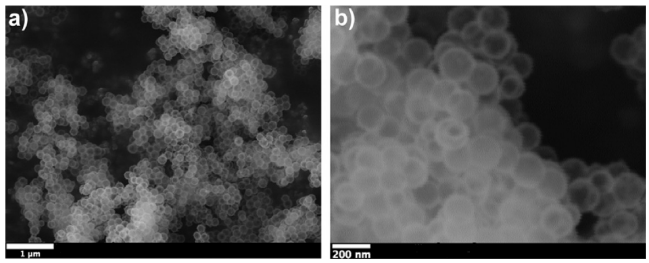

Figure 1. SEM images of 200 nm Fe-doped, SiO_2 calcined nanoshells. SEM images of iron(III)-doped, silica nanoshells. The PS template was removed during the calcination process. The scale bars are (a) 1 μm and (b) 200 nm (0.2 μm).

dx.doi.org/10.1021/ja3036114 | J. Am. Chem. Soc. 2012, 134, 13997−14003

the DLS fitting parameters and the SEM images suggested problems due to the iron-doped, silica nanoshells absorbing the laser (633 nm) used in DLS thereby distorting the size measurements. In order to better characterize the dispersed nanoshells in solution, wet SEM capsules, from QuantoMix, were used to directly image the particles dispersed in water (Figure 2). The nanoshells imaged using the wet SEM capsules

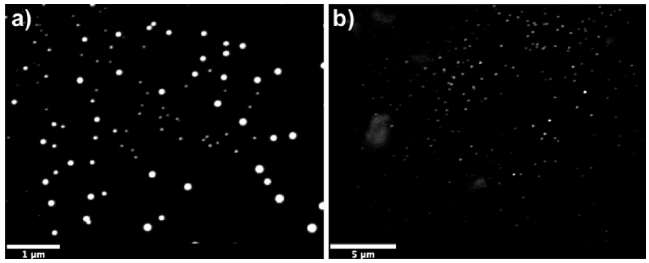

Figure 2. Wet SEM images of calcined, 200 nm Fe-doped, SiO_2 nanoshells. Nanoshells were suspended in water and placed in a QuantoMix wet SEM capsule for imaging. The scale bars are (a) 1 and (b) 5 μm.

appear to be predominantly single, 180 nm particles. The images also show particles that appear to be smaller in size. The apparent size range is due to the increased distance between the particles and the capsule membrane. The SEM images in Figure 1 on a flat substrate show that the individual nanoshells are uniform in size.

The iron content of the Fe-doped, silica nanoshells was determined using EDS and inductively coupled plasma optical emission spectroscopy (ICP-OES). EDS measurements were obtained for 20 different frames and 3 different samples during SEM imaging. The mole percent (mol %) values were then averaged. The expected mol % for iron, from the fraction added during synthesis, is 4.7%. EDS of the Fe(III)-doped nanoshells shows a mol % of 5.7 ± 1.8%.

ICP-OES was used as a bulk analysis method to quantify the amount of iron doped into the silica nanoshells. A 1 mg portion of Fe(III)-doped, silica nanoshells was suspended in 10 mL of 2% nitric acid. The ICP optical emission spectrum was measured at five wavelengths (see Experimental section), and the resulting concentrations were averaged. The dilution factor was corrected by multiplying the averaged value by 100. The 1 mg of particles suspended in 1 mL of solution should produce an iron concentration of 0.83 mM (4.7 mol %). After correcting for the dilution of the particles, the concentration of iron in the nanoshells was determined to be 0.72 ± 0.04 mM (~4.1 ± 0.2 mol %). It can be concluded that approximately 88% of the added iron(III) ethoxide used in the synthesis reaction is incorporated into the nanoshell. This is also the maximum amount of iron that can be incorporated into the nanoshell without adversely affecting its strength, as attempts to introduce higher amounts of iron(III) ethoxide in the synthesis led to the formation of colloidal matter and broken nanoshells.

The EPR spectrum at 77 K showed no appreciable signal, suggesting that the iron present in the nanoshells is antiferromagnetically coupled.[35,36] Bulk magnetic susceptibility measurements were performed. Mass susceptibility measurements, χ_g, were plotted as χ_g^{-1} vs the absolute temperature (a Curie–Weiss plot, see Supporting Information). The data closely follow Curie behavior, as evidenced by the linearity of the data to low temperatures. The Weiss temperature was determined to be −10.5 K. The negative Weiss temperature suggests that the iron(III) in the nanoshells is weakly antiferromagnetically coupled to other iron(III) centers within the nanoshell or between individual particles.[37,38] This observation agrees with the EPR results. Antiferromagnetic behavior of iron(III) doped into silica has also been observed in silica films and attributed to the presence of small iron nanoparticles.[39] This suggests a heterogeneous structure where small clusters of hydrated iron(III) oxide and silica gel are fused together on the template surface during nanoshell formation.[38,39]

Small Molecule Chelation and Degradation of Iron-(III)-Doped, SiO_2 Nanoshells. Small molecule chelation was initially used to determine whether nanoshell degradation could be promoted by iron removal. Deferiprone, EDTA, and desferrioxamine were used because of their known high affinity for iron(III) as well as their use as metal chelation therapy agents. EDTA strongly binds iron(III) with a formation constant of ~10.[25] Its high binding affinity and use in a variety iron(III) chelating applications made it a suitable compound for this study. Desferrioxamine and deferiprone were investigated because of their therapeutic use to treat iron overload in patients. Desferrioxamine mesylate (desferal) is FDA approved to treat individuals with iron overload disorders, such as hemochromatosis or thalassemia. It chelates iron(III) with a binding constant of 10.[30] Desferrioxamine (desferal) is ususally administered intravenously due to its low absorption in the gastrointestinal tract. Deferiprone (ferriprox) is used in Europe as an alternative, orally administered, iron overload treatment and has a iron(III) binding constant of 10.[20]

Desferrioxamine and deferiprone both form orange colored solutions after binding iron(III). This allows colorimetric quantification of iron removal from the nanoshells. Figure 3a shows the supernatant from the nanoshell degradation using deferiprone as the chelating agent. The procedure for nanoshell degradation is provided in detail in the Experimental section. As seen in Figure 3, the color intensity of the supernatant decreases over time thus indicating that less iron is being removed with successive extractions. It should be noted that the nanoshell pellet isolated from the supernatant also becomes paler as the iron is removed. The solid pellet also decreases in size and is more difficult to isolate, by centrifugation, over time as the nanoshells dissolve. Iron(III)-doped, SiO_2 nanoshells were submerged in Milli-Q water and DPBS, without $CaCl_2$, and incubated at 80 °C as a control. No change was observed in the color of the supernatant or in the morphology of the nanoshells after 7 days, indicating that a chelating agent is required for the removal of iron from the nanoshells. Adding deferiprone to the supernatant failed to produce any colorimetric response for iron(III), visually or spectrophotometrically.

These result establish that small molecule chelation can be used to remove iron(III) from the nanoshells and cause their breakdown into soluble species. The total amount of iron removed, Figure 3b, by the three chelating agents is approximately equal to the amount of iron incorporated into the nanoshells as determined by EDS and ICP-OES.

The results from Figure 3b show that 57%, 39%, and 42% of the iron doped into the nanoshells is removed after 24 h exposure to EDTA, desferrioxamine, and deferiprone, respectively. Desferrioxamine has the largest formation constant yet removes the smallest amount of iron in the first 24 h period relative to EDTA and deferiprone. Compared to EDTA and deferiprone, desferrioxamine is the largest molecular weight

dx.doi.org/10.1021/ja3036114 | J. Am. Chem. Soc. 2012, 134, 13997–14003

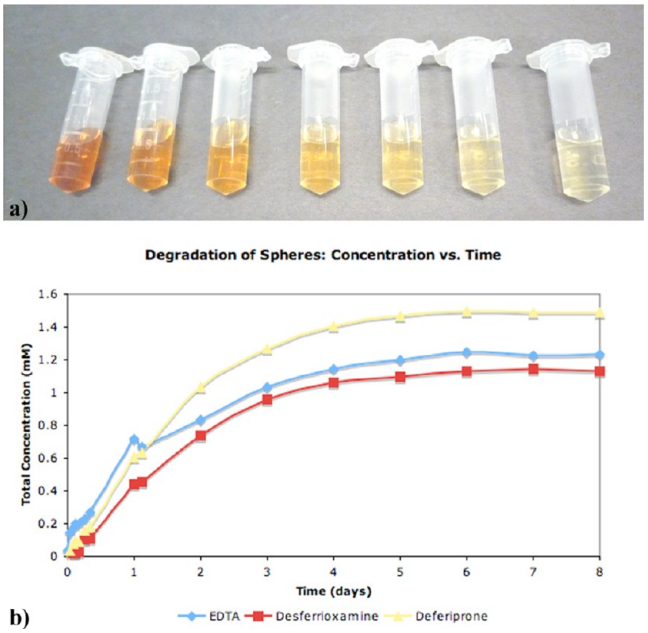

Figure 3. Small molecule chelation of Fe(III) in Fe-doped, SiO_2 nanoshells. In 1 mL of 0.1 M aqueous chelating solution (EDTA, desferrioxamine, or deferiprone), 1 mg of 200 nm iron(III)-doped, SiO_2 nanoshells was submerged. The supernatant was removed and analyzed by UV–vis spectroscopy every 24 h. (a) The photographic image on the top shows the color intensity of the aliquots of Fe–deferiprone complex extracted over 7 d. (b) The graph shows the cumulative concentration of Fe(III) removed from the nanoshells on chelation by EDTA, desferrioxamine, and deferiprone (blue, red, and yellow curves, respectively).

chelator and must fold appropriately in order to bind the iron in an octahedral complex. As a result, the process of removing iron appears to be kinetically hindered during the first 24 h. EDTA is the next largest of the chelators but is able to readily form the octahedral complex due to its compact structure. The minimal required reorganization of EDTA, along with its high formation constant, lead to the increased removal rate of iron from the nanoshells within the first 24 h. Deferiprone is not only the smallest of the chelators used but also has the lowest formation constant of the three. It has ready steric access to the iron in the nanoshells; however, because of its lower formation constant, it does not remove as much iron as EDTA within the first 24 h period. There are obvious differences in the rate of iron removal in the first 24 h period, yet approximately 84% of the iron(III) doped into the nanoshells is removed after exposure to the iron chelates for 3 days, regardless of the type of chelator.

It can therefore be concluded that the chelating agents are removing all the iron in the nanoshells. The decreased yield of recoverable nanoshells as the iron is removed suggests that the chelated iron comes from a structural site, thereby leading to the collapse and dispersal of the nanoshell into smaller, soluble fragments.

The collapse of the nanoshell structure was examined using deferiprone to chelate the iron. The SEM images, seen in Figure 4, show thinning of the nanoshell wall as iron is removed, collapse of the structure, and the presence of colloidal silica as iron is removed in stages until no colloidal silica is recoverable by centrifugation. Thinning of the nanoshell wall is observed during the first 3 days of exposure of the iron(III)-doped nanoshells to the chelating solutions. No holes are

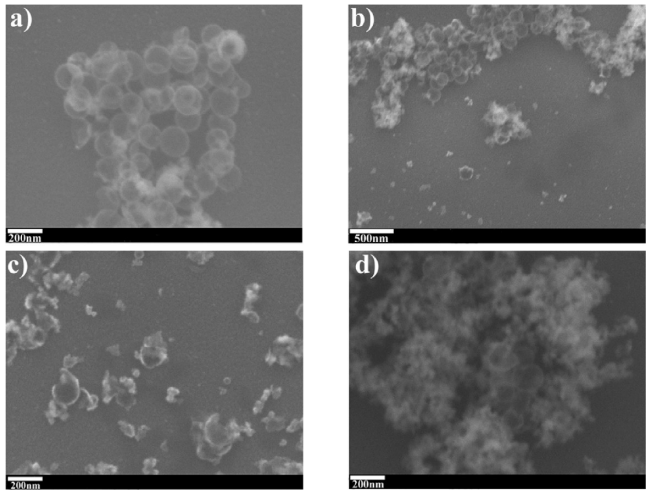

Figure 4. Degradation of 200 nm Fe-doped, silica nanoshells using deferiprone. Collapse of the nanoshell structure, imaged by SEM, as iron is removed, via deferiprone chelation, over (a) 0, (b) 1, (c) 3, and (d) 7 days. The haze observed in panel d was determined by EDS to be primarily colloidal silica.

observed in the TEM images of the parent nanoshells (see Supporting Information), indicating that the pores in the silica are <1 nm in diameter. Given the small dimensions of the pores, the chelate may slowly diffuse within the pores, thus the iron may be removed preferentially from the outer surface of the nanoshell. As iron is removed from the outer surface, the walls of the nanoshells become thinner until the structure begins to collapse (Figure 4c). After the nanoshell ruptures, the chelates should have better access to both surfaces of the nanoshell leading to enhanced iron removal and the production of colloidal silica (the haze seen in Figure 4d).

These results show that doping ferric iron into silica during the sol–gel synthesis results in a material that even after calcination can be degraded by removal of iron(III). The degradation seen using chelates, such as desferrioxamine, an FDA approved drug, and deferiprone, suggests a potential method for removing iron(III)-doped silica from living organisms. The next test was to determine whether iron-sequestering proteins present in mammalian serum, such as transferrin, would be able to remove the iron(III) from the nanoshells and promote biodegradation.

Degradation of Iron(III)-Doped, SiO_2 Nanoshells in Mammalian Serum. Small molecule chelation experiments show that iron removal resulted in the collapse of the iron(III)-doped, silica nanoshell structure with eventual dissolution to noncentrifugable fragments. To determine whether the biological ligands for iron(III) present in serum could affect a similar degradation process under conditions relevant to *in vivo* dosing, the biodegradability of the iron(III)-doped, silica nanoshells was tested by immersing them in serum. Serum, the liquid portion of blood with the cells and clotting factors removed, contains the iron(III) chelating protein transferrin. Its high binding constant, 10,[20] is similar to that of the small molecule chelators used in the preliminary study. Therefore, it seemed likely that the binding of iron(III) by transferrin should also lead to the collapse and dissolution of the nanoshell structure.

Figure 5 displays SEM images of 200 nm silica nanoshells, which serve as a control, and iron(III)-doped, silica nanoshells that have been immersed in FBS and HS for various time

dx.doi.org/10.1021/ja3036114 | J. Am. Chem. Soc. 2012, 134, 13997–14003

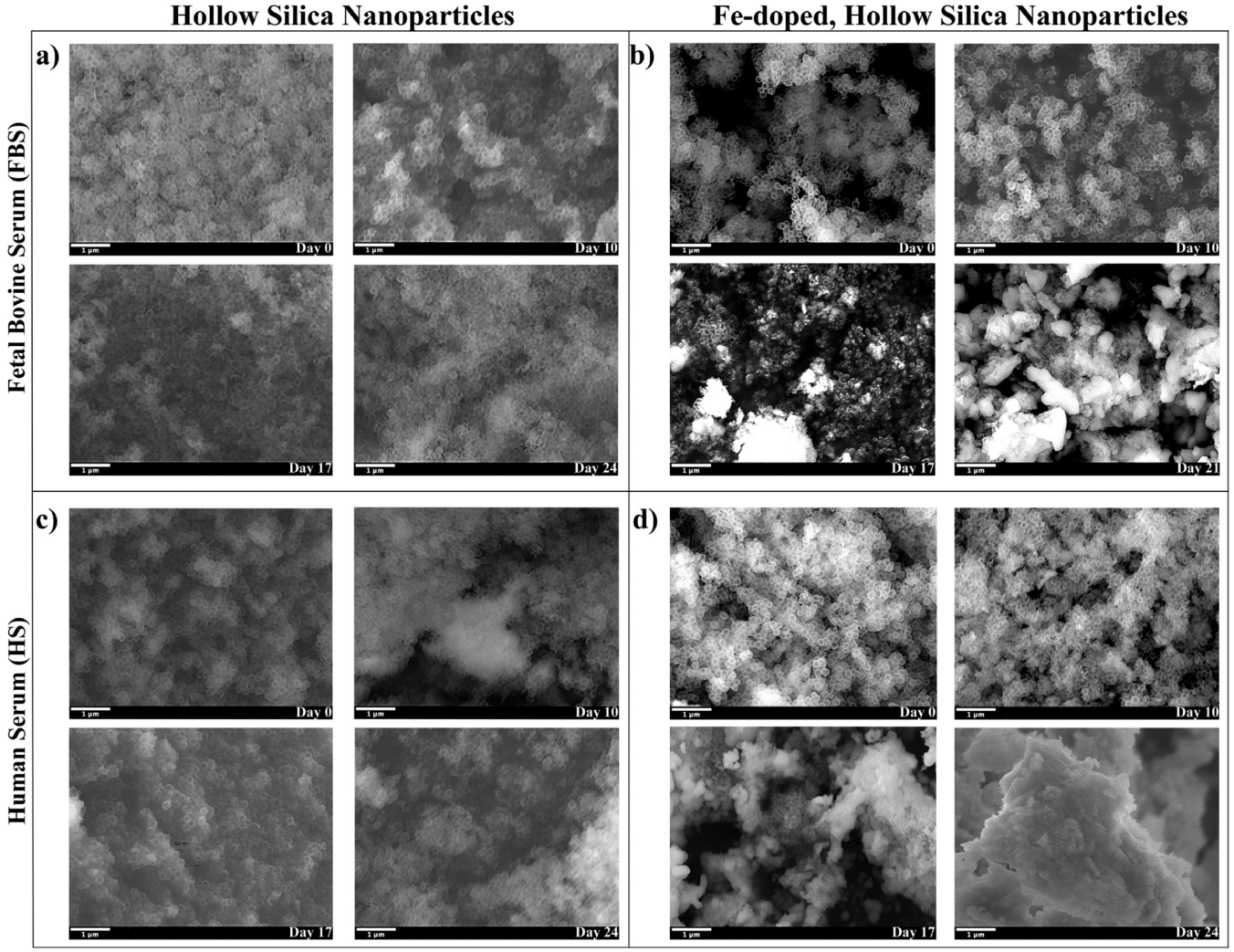

Figure 5. SEM images of nanoshell degradation in FBS and HS. Silica nanoshells serve as degradation controls in (a) FBS and (c) HS compared to ~5% iron(III)-doped, silica nanoshells in (b) FBS and (d) HS. Images in (a) and (c) show the morphology of the nanoshells on exposure to serum at 37 °C after 0, 10, 17, and 24 days.

periods. The samples were incubated at 37 °C (physiological temperature), and images were taken of the pellet that was isolated at different time points. As seen in Figure 5a,c, the undoped silica nanoshells remain intact in both FBS and HS over the course of 24 days and are easy to isolate via centrifugation. It should be noted that the last images of the plain silica nanoshells are shown at day 24 for comparison to iron(III)-doped, silica nanoshells. However, the plain silica nanoshells remain intact after 24 days, confirming the inertness of calcined silica. The slight haze that appears as time progresses is due to small amounts of serum salts, such as NaCl and $CaCl_2$, which were confirmed using EDS.

When comparing the 200 nm iron(III)-doped, silica nanoshells, seen in Figure 5b,d, to the control undoped silica nanoshells it is apparent that the results differ markedly. Although there are many imageable, intact nanoshells at 10 days, 7 days later it becomes difficult to find any nanoshells, and only irregular solid fragments are seen. The EDS analysis, seen in Tables S1 and S2 (Supporting Information), showed that these solids contain large fractions of calcium and phosphorus, which can be attributed to remineralization of the iron-doped silica with the calcium phosphate present in serum after breakdown and dissolution of the iron(III)-doped, silica nanoshells.

The silicon content measured using EDS (see Tables S1 and S2, Supporting Information) also decreases as the amount of calcium and phosphorus increases. The iron(III)-doped, silica nanoshells dispersed in FBS could only be isolated, via centrifugation, up to 21 days. The pellet that was obtained from FBS at 21 days was <1% of the initial amount of nanoshells, of which the entire recovered sample was imaged. Of the sample that was imaged, it was not possible to find any nanoshells. Only fragments primarily composed of calcium and phosphorus were in the recovered solid. The same trend is seen for the iron(III)-doped, silica nanoshells that had been immersed in HS; however, the last pellet that could be isolated was at 24 days rather than after 21 days. Again, <1% of the original sample weight was recoverable by centrifugation after 24 days, and again the isolable solid particles were high in calcium and phosphorus, which is indicative of extensive remineralization of the silica.

There was not a similar significant increase in the amount of measured calcium and phosphorus in the undoped silica control samples. The increased amount of calcium and phosphorus seen in the iron(III)-doped, silica nanoshells is attributed to the

dx.doi.org/10.1021/ja3036114 | J. Am. Chem. Soc. 2012, 134, 13997−14003

degradation of the nanoshells into smaller, soluble fragments and subsequent remineralization with the soluble calcium(II) and phosphate ions present in serum, yielding tiny amounts of a mixed calcium phosphate silicate.[20,22,25,27,40] The iron(III)-doped, silica nanoshells have to degrade for at least 17 days at physiological conditions before degradation is observed by SEM. After 21−24 days, the trace solid that was recovered and imaged by SEM images consists chiefly of calcium phosphate, and very low levels of silica are detected. It has been observed previously that the formation of calcium phosphate depends on its ability to crystallize at a silica surface.[22] These results strongly suggest that the iron in the nanoshell structure can be removed by iron sequestering proteins found in serum leading to the collapse of the structure and the formation of molecular or extremely small silica clusters that cannot be recovered by centrifugation.

■ CONCLUSION

It has been demonstrated that iron(III) can be doped into a silica nanoshell during sol−gel synthesis. Incorporation of iron(III) into the silica matrix was shown to make the nanoshells degradable in the presence of iron chelating agents. The biodegradability of the nanoparticles under conditions relevant to *in vivo* use was demonstrated through their solubilization in FBS and HS after approximately 20−25 days at physiological temperature. This approach provides a general method to make porous, calcined silica biodegradable and may enable broad application of silica nanoparticles in biomedical technologies.[41,42]

■ ASSOCIATED CONTENT

Supporting Information

ICP-OES methods for sample preparation and quantification of iron in nanoshells; methods for preparation of sample for magnetic susceptibility measurements; Curie−Weiss plot of mass susceptibility vs temperature; DLS and ζ potential measurements of 200 nm iron(III)-doped, hollow silica nanoshells; and tabulated EDS data of degradation of plain silica and iron(III)-doped, silica nanoshells; control images of iron(III)-doped, silica nanoshells in water; TEM images of 200 nm iron(III)-doped, silica nanoshells. This material is available free of charge via the Internet at http://pubs.acs.org.

■ AUTHOR INFORMATION

Corresponding Author

wtrogler@ucsd.edu

Notes

The authors declare no competing financial interest.

■ ACKNOWLEDGMENTS

The project described was supported by award number P42ES010337 from the National Institute of Environmental Health Sciences and NIH grant U54 CA 119335. The content is solely the responsibility of the authors and does not necessarily represent the official views of the National Institute of Environmental Health Sciences or the National Institutes of Health. We acknowledge the use of the UCSD Cryo-Electron Microscopy Facility which is supported by NIH grants to Dr. Timothy S. Baker and a gift from the Agouron Institute to UCSD. We also thank the Scripps Institution of Oceanography Analytical Facility (ICP-OES), Prof. Michael Tauber and Dr. Hannah Shafaat at the University of California San Diego (UCSD) for performing the EPR measurements, and Prof. David Hendrickson, Dr. Christopher Beedle, and Dr. Katie Heroux for collecting and aiding in the analysis of the dc magnetic susceptibility data. A.L. is supported by an R25 CA153915 training grant as well as R01CA095298 from the National Cancer Institute. K. K.P.M. thanks the UCSD Socrates Program for an NSF GK-12 STEM fellowship.

■ REFERENCES

(1) Arnal, P. M.; Comotti, M.; Schueth, F. *Angew. Chem., Int. Ed.* **2006**, *45* (48), 8224−8227.
(2) Jin, P.; Chen, Q.; Hao, L.; Tian, R.; Zhang, L.; Wang, L. *J. Phys. Chem. B* **2004**, *108* (20), 6311−6314.
(3) Martinez, H. P.; Kono, Y.; Blair, S. L.; Sandoval, S.; Wang-Rodriguez, J.; Mattrey, R. F.; Kummel, A. C.; Trogler, W. C. *MedChemComm* **2010**, *1*, 266−270.
(4) Slowing, I. I.; Trewyn, B. G.; Giri, S.; Lin, V. S. Y. *Adv. Funct. Mater.* **2007**, *17* (8), 1225−1236.
(5) Slowing, I. I.; Trewyn, B. G.; Lin, V. S. Y. *J. Am. Chem. Soc.* **2007**, *129* (28), 8845−8849.
(6) Wang, H.; Yang, Z. Y.; Lu, Y. F. *J. Appl. Phys.* **2007**, *101* (3), 033129/1−033129/5.
(7) Xu, X.; Asher, S. A. *J. Am. Chem. Soc.* **2004**, *126* (25), 7940−7945.
(8) Zhu, Y.; Shi, J.; Shen, W.; Dong, X.; Feng, J.; Ruan, M.; Li, Y. *Angew. Chem., Int. Ed.* **2005**, *44* (32), 5083−5087.
(9) Alexis, F.; Pridgen, E.; Molnar, L. K.; Farokhzad, O. C. *Mol. Pharmaceutics* **2008**, *5* (4), 505−515.
(10) He, Q.; Shi, J. *J. Mater. Chem.* **2011**, *21*, 5845−5855.
(11) He, X.; Nie, H.; Wang, K.; Tan, W.; Wu, X.; Zhang, P. *Anal. Chem. (Washington, DC, U. S.)* **2008**, *80* (24), 9597−9603.
(12) Huang, X.; Li, L.; Liu, T.; Hao, N.; Liu, H.; Chen, D.; Tang, F. *ACS Nano* **2011**, *5* (7), 5390−9.
(13) Barbe, C.; Bartlett, J.; Kong, L.; Finnie, K.; Lin, H. Q.; Larkin, M.; Calleja, S.; Bush, A.; Calleja, G. *Adv. Mater. (Weinheim, Ger.)* **2004**, *16*, 1959−1966.
(14) Lee, C.-H.; Cheng, S.-H.; Wang, Y.-J.; Chen, Y.-C.; Chen, N.-T.; Souris, J.; Chen, C.-T.; Mou, C.-Y.; Yang, C.-S.; Lo, L.-W. *Adv. Funct. Mater.* **2009**, *19* (2), 215−222.
(15) Lu, J.; Liong, M.; Li, Z.; Zink, J. I.; Tamanoi, F. *Small* **2010**, *6*, 1794−1805.
(16) Chen, Y.; Chen, J.; Dong, J.; Jin, Y. *Toxicol. Ind. Health* **2004**, *20*, 21−7.
(17) Han, B.; Guo, J.; Abrahaley, T.; Qin, L.; Wang, L.; Zheng, Y.; Li, B.; Liu, D.; Yao, H.; Yang, J.; Li, C.; Xi, Z.; Yang, X. *PLoS One* **2011**, *6*, e17236.
(18) Napierska, D.; Thomassen, L. C. J.; Lison, D.; Martens, J. A.; Hoet, P. H. *Part. Fibre Toxicol.* **2010**, *7*, 39.
(19) Andersson, J.; Rosenholm, J.; Areva, S.; Linden, M. *Chem. Mater.* **2004**, *16* (21), 4160−4167.
(20) Kortesuo, P.; Ahola, M.; Karlsson, S.; Kangasniemi, I.; Kiesvaara, J.; Yli-Urpo, A. *J. Biomed. Mater. Res.* **1999**, *44*, 162−167.
(21) Kortesuo, P.; Ahola, M.; Karlsson, S.; Kangasniemi, I.; Yli-Urpo, A.; Kiesvaara, J. *Biomaterials* **2000**, *21*, 193−8.
(22) Li, P.; Ohtsuki, C.; Kokubo, T.; Nakanishi, K.; Soga, N.; Nakamura, T.; Yamamuro, T. *J. Am. Ceram. Soc.* **1992**, *75* (8), 2094−7.
(23) Lee, E.-J.; Teng, S.-H.; Jang, T.-S.; Wang, P.; Yook, S.-W.; Kim, H.-E.; Koh, Y.-H. *Acta Biomater.* **2010**, *6* (9), 3557−3565.
(24) Radin, S.; El-Bassyouni, G.; Vresilovic, E. J.; Schepers, E.; Ducheyne, P. *Biomaterials* **2005**, *26*, 1043−52.
(25) Radin, S.; Falaize, S.; Lee, M. H.; Ducheyne, P. *Biomaterials* **2002**, *23*, 3113−3122.
(26) Seleem, M. N.; Munusamy, P.; Ranjan, A.; Alqublan, H.; Pickrell, G.; Sriranganathan, N. *Antimicrob. Agents Chemother.* **2009**, *53* (10), 4270−4274.
(27) Vaekiparta, M.; Jokinen, M.; Vaahtio, M.; Vallittu, P. K.; Yli-Urpo, A. *Key Eng. Mater.* **2004**, *254−256*, 553−556.

(28) Xue, J. M.; Tan, C. H.; Lukito, D. *J. Biomed. Mater. Res., Part B* **2006**, *78B* (2), 417−422.
(29) Jokinen, M.; Peltola, T.; Veittola, S.; Rahiala, H.; Rosenholm, J. B. *J. Eur. Ceram. Soc.* **2000**, *20* (11), 1739−1748.
(30) Li, X.; Zhang, L.; Dong, X.; Liang, J.; Shi, J. *Microporous Mesoporous Mater.* **2007**, *102* (1−3), 151−158.
(31) Bertini, I.; Gray, H. B.; Stiefel, E. I.; Valentine, J. S. *Biological Inorganic Chemistry: Structure and Reactivity*; University Science Books: Sausalito, CA, 2007; p 739.
(32) Crichton, R. R.; Charloteaux-Wauters, M. *Eur. J. Biochem.* **1987**, *164* (3), 485−506.
(33) Yang, J.; Lind, J. U.; Trogler, W. C. *Chem. Mater.* **2008**, *20* (9), 2875−2877.
(34) Trogler, W. C.; Esener, S. C.; Messmer, D.; Lind, J. U.; Pohaku, K.; Yang, J. Hollow silica nanospheres for drug delivery and gene transfer. *PCT Int. Appl.*, WO 2009023697, 2009, pp 76.
(35) Tanaka, K.; Kamiya, K.; Matsuoka, M.; Yoko, T. *J. Non-Cryst. Solids* **1987**, *94* (3), 365−373.
(36) Yanez-Limon, J. M.; Perez-Robles, J. F.; Gonzalez-Hernandez, J.; Vorobiev, Y. V.; Romano, J. A.; Gandra, F. C. G.; Da, S. E. C. *J. Sol-Gel Sci. Technol.* **2000**, *18* (3), 207−217.
(37) Carlin, R. L. *Magnetochemistry*; Springer-Verlag: Berlin, Heidelberg, Germany, 1986.
(38) Heinrichs, B.; Rebbouh, L.; Geus, J. W.; Lambert, S.; Abbenhuis, H. C. L.; Grandjean, F.; Long, G. J.; Pirard, J.-P.; van Santen, R. A. *J. Non-Cryst. Solids* **2008**, *354* (2−9), 665−672.
(39) Babonas, G. J.; Reza, A.; Simkiene, I.; Sabataityte, J.; Baran, M.; Szymczak, R.; Karlsson, U. O.; Suchodolskis, A. *Appl. Surf. Sci.* **2006**, *252* (15), 5391−5394.
(40) Jokinen, M.; Peltola, T.; Veittola, S.; Simola, J.; Yli-Urpo, A. *Key Eng. Mater.* **2002**, *218−220* (Bioceramics-14), 283−286.
(41) Martinez, H. P.; Kono, Y.; Blair, S.; Mattrey, R.; Kummel, A. C.; Trogler, W. C. *Med. Chem. Commun.* **2012**, *1*, 266−270.
(42) Liberman, A.; Martinez, H. P.; Ta, C. N.; Barback, C. V.; Mattrey, R. F.; Kono, Y.; Blair, S. L.; Trogler, W. C.; Kummel, A. C.; Wu, Z. *Biomaterials* **2012**, *33*, 5124−5129.